International Journal of Solids and Structures 51 (2014) 392–401

Contents lists available at ScienceDirect

International Journal of Solids and Structures

journal homepage: www.elsevier.com/locate/ijsolstr

Construction of multi-dimensional isotropic kernels for nonlocal elasticity based on phonon dispersion data

Susanta Ghosh *, Veera Sundararaghavan [1], Anthony M. Waas [2]

University of Michigan, Ann Arbor, USA

ARTICLE INFO

Article history:
Received 29 March 2013
Received in revised form 9 August 2013
Available online 18 October 2013

Keywords:
Isotropic
Nonlocal
Elasticity
Kernel
Phonon dispersion
Axisymmetry
Hankel transform
Lattice dynamics

ABSTRACT

Kernels for non-local elasticity are in general obtained from phonon dispersion relations. However, non-local elastic kernels are in the form of three-dimensional (3D) functions, whereas the dispersion relations are always in the form of one-dimensional (1D) frequency versus wave number curves corresponding to a particular wave direction. In this paper, an approach to build 2D and 3D kernels from 1D phonon dispersion data is presented. Our particular focus is on isotropic media where we show that kernels can be obtained using Fourier–Bessel transform, yielding axisymmetric kernel profiles in reciprocal and real spaces. These kernel functions are designed to satisfy the necessary requirements for stable wave propagation, uniformity of nonlocal stress and stress regularization. The proposed concept is demonstrated by developing some physically meaningful 2D and 3D kernels that will find useful applications in nonlocal mechanics. Relative merits of the kernels obtained via proposed methods are explored by fitting 1D kernels to dispersion data for Argon and using the kernel to understand the size effect in non local energy as seen from molecular simulations. A comparison of proposed kernels is made based on their predictions of stress field around a crack tip singularity.

1. Introduction

Theories of classical continuum mechanics which relate local strain to work-conjugate local stress measures, provide length-scale independent solutions, and are successful in addressing a large number of physical problems. However, these theories are found to be deficient for several situations that require a characteristic length scale of the medium to enter in the physical solution. Examples include stress and strain fields around sharp crack-tips, wave dispersion, strain softening and attendant size effects (see for example, Bažant and Cedolin, 2010). The fact that atomistic calculations of material properties are necessarily non-local in their construction, upscaling from an atomistic model to a continuum model would lead to continuum stress–strain relations that display non-local character. Nonlocal theories and their implementations have been intensely researched due to their promise in capturing non-local atomistic phenomena, however, the understanding developed to-date is incomplete. Several review articles, (Bažant and Jirásek, 2002; Aifantis, 2003; Askes and Aifantis, 2011; Maugin and Metrikine, 2010) have provided important details and much insight into the types of non-local continuum theories that are at our disposal. There exists varieties of nonlocal theories depending on the strategies to incorporate additional atomistic features. The focus of the present paper is on the integral type nonlocal theory proposed in (Eringen, 1983).

In the integral type nonlocal theory, the stress at a material point is related to a weighted integral of strains over a certain finite neighborhood. The weighting function (α) is the non-local *kernel*. The nonlocal stress, $\boldsymbol{t}$, in a linear elastic body, V, can be described as,

$$t_{ij}(\boldsymbol{x}) = \int_{\Omega} \alpha_{ijkl}(\boldsymbol{x},\boldsymbol{x}')\epsilon_{kl}(\boldsymbol{x}')\,d\Omega \tag{1}$$

where $\boldsymbol{\alpha}$ is a tensorial kernel representing an attenuating elastic modulus. Here, $\boldsymbol{t}$ and $\boldsymbol{\epsilon}$ are the nonlocal stress and local strain tensors, respectively, $\Omega \subset V$ is the compact support for the kernel and $\boldsymbol{x}$ and $\boldsymbol{x}'$ are position vectors for two material points in Ω. In isotropic media, it is assumed that a unique kernel weights all entries of the stiffness tensor equally (Eringen, 2002), and the above equation becomes,

$$t_{ij}(\boldsymbol{x}) = \int_{\Omega} \alpha(\boldsymbol{x},\boldsymbol{x}')C_{ijkl}\epsilon_{kl}(\boldsymbol{x}')\,d\Omega = \int_{\Omega} \alpha(\boldsymbol{x},\boldsymbol{x}')\sigma_{ij}(\boldsymbol{x}')\,d\Omega \tag{2}$$

Here, $\boldsymbol{\sigma}$ is the Hookean (local) stress tensor, C_{ijkl} is the stiffness tensor for an isotropic material and α is a *scalar kernel function*. In

* Corresponding author. Currently a Research Fellow of Materials Science and Engineering.
E-mail addresses: susantag@umich.edu (S. Ghosh), veeras@umich.edu (V. Sundararaghavan), dcw@umich.edu (A.M. Waas).
[1] Assistant Professor of Aerospace Engineering.
[2] Felix Pawlowski Collegiate Professor of Aerospace Engineering; visiting Professor, Department of Aeronautics, Imperial College, London.

0020-7683/$ - see front matter © 2013 Elsevier Ltd. All rights reserved.
http://dx.doi.org/10.1016/j.ijsolstr.2013.10.004

general, the following additional properties are attributed to the kernel function, α, as described in (Eringen, 1983),

- The kernel has a peak at $\|\boldsymbol{x}-\boldsymbol{x}'\|=0$, and decays with increasing distance $\|\boldsymbol{x}-\boldsymbol{x}'\|$.
- The kernel function α reverts to a delta function as the non local zone of influence vanishes, i.e., as $\lim_{\Omega\to 0}\alpha=\delta$. As such, $\alpha(\boldsymbol{x},\boldsymbol{x}')$ satisfies the normalization condition, i.e., $\int_\Omega \alpha(\boldsymbol{x},\boldsymbol{x}')\,d\Omega=1$.
- α is bi-symmetric, i.e., $\alpha(\boldsymbol{x},\boldsymbol{x}')=\alpha(\boldsymbol{x}',\boldsymbol{x})$ and function of $\boldsymbol{x}-\boldsymbol{x}'$.

Additionally, Bažant and Chang (1984) suggested that a continuum should not yield zero energy modes for non-rigid-body deformations and should have real wave propagation velocity, which requires that the Fourier transform of α have positive values all over the reciprocal space. The same restriction on α has been reached in Polizzotto (2001) by noting that Eq. (2) is a homogeneous Fredholm integral equation of first kind and then invoking the Fredholm integral equation theory. It is noted in Bažant and Chang (1984) that some of the popular kernels do not satisfy the required conditions. Thus, it is suggested to include a dirac delta function to alleviate this problem. However, the inclusion of a delta function leads to the loss of stress regularity property of nonlocal elasticity whenever the local stress is singular. In contrast to the above mentioned restrictions on the kernel, recent research through molecular simulations have indicated that at the nanoscale, the kernel α attenuation need not be monotonous (Picu, 2002; Sundararaghavan and Waas, 2011). The reason for α to be non-monotonous is attributed to the similarity between non-local kernels and inter-atomic potentials (Picu, 2002; Sundararaghavan and Waas, 2011). The normalization condition suggests that for all $\Omega\subset V$ a uniform local strain field would produce a uniform nonlocal stress field. However, we point out that this particular restriction of nonlocal kernel is meant to be satisfied as long as Ω does not intersect the boundary ∂V of the body V. Violation of the normalization requirement leads to various problems, for instance, when Ω intersects ∂V, a uniform strain yields a non-uniform nonlocal stress. From a purely mathematical perspective, few modifications to the kernel (Polizzotto, 2001; Borino et al., 2003; Polizzotto et al., 2004) have been suggested in the past in order to satisfy the normalization requirement at domain boundaries. Notwithstanding the symmetry achieved in these papers, we note that the symmetry condition of any function is determined by symmetry of its domain and codomain. Since, near the boundary $\Omega\not\subset V$, the domain of α itself is not symmetric with respect to the center of Ω. Hence, the symmetry conditions near the boundary may need further investigation. For detailed description about the properties of the kernel function, the reader is referred to Eringen (1983), Bažant and Chang (1984), Bažant and Jirásek (2002), Polizzotto (2001) and Ghosh et al. (2013).

While various studies have focused on (mostly macroscopic) nonlocal continuum and their numerical implementations, only a few have focused on the connection of these theories to realistic materials at small scale (Lam et al., 2003; Han, 2010, and references therein). The various additional (length scale) parameters or kernels needed to capture the non-locality of the material can be obtained via molecular simulations (Picu, 2002; Maranganti and Sharma, 2007a). A systematic attempt at generating 3D kernels from molecular simulations is developed in Picu (2002). However, the 3D kernels are not defined for distances below the distance at which the *radial distribution function* goes to zero, and were constructed only for pairwise potentials. For general interatomic potentials, the nonlocality is commonly obtained via wave dispersion studies. The dispersion curves are obtained for wave modes propagating along specific wave vectors. The dispersion curves obtained in this manner are inherently one dimensional, whereas for analyzing continua (represented via integral type nonlocality) multi-dimensional kernels are needed. In this paper, a new and general procedure to obtain 2D and 3D isotropic nonlocal kernels from dispersion data is proposed. Our particular focus is on isotropic media, where we show that kernels obtained using Fourier–Bessel transform, yield axisymmetric kernel profiles in reciprocal or real space. These kernels satisfy the necessary requirements for stable wave propagation, and uniformity of nonlocal stress and stress regularization. The proposed concept is demonstrated using physically meaningful 2D and 3D kernels that should find useful applications in nonlocal mechanics.

2. Integral-type nonlocal elasticity

The equations of motion for a non-local medium is given by,

$$t_{ij,i}+\rho(f_j-\ddot{u}_j)=0 \tag{3}$$

where $t_{ij}=C_{ijkl}\int_\Omega \alpha(\boldsymbol{x}-\boldsymbol{x}')\epsilon_{kl}(\boldsymbol{x}')\,d\Omega$ for an isotropic medium. It is experimentally observed that bulk and surface waves experience wave dispersion at higher frequencies, i.e., the phase velocity depends on the wavelength. The theories of lattice dynamics can demonstrate this dispersion behavior (see Dove, 1993) but classical elasticity fails to do the same. The following steps recapitulate that nonlocal elasticity can represent wave dispersion through the kernel function. Consider a plane wave solution for an infinite nonlocal solid with no body force: $u_j(\boldsymbol{x},t)=A_j e^{i(\boldsymbol{k}\cdot\boldsymbol{x}-\omega t)}$, where $\boldsymbol{k}$ and ω are the angular wave vector and the angular frequency respectively. Substituting u_j in the equilibrium equation, Eq. (3), yields:

$$|\rho\omega^2\delta_{jk}-C_{ijkl}\hat{\alpha}(\boldsymbol{k})k_ik_l|=0 \tag{4}$$

here $\hat{\alpha}(\boldsymbol{k})$ denotes the Fourier transformed kernel. The phonon dispersion relation relating the angular frequency ω and the wave number $k=\|\boldsymbol{k}\|$ is given by Eq. (4). For isotropic case ($C_{ijk\ell}=\lambda\delta_{ij}\delta_{k\ell}+\mu(\delta_{ik}\delta_{j\ell}+\delta_{i\ell}\delta_{jk})$) in which λ and μ denote the Lame' constants, the above equation reduces to the following:

$$\rho\,\omega^2=(\lambda+2\mu)\,\hat{\alpha}(\boldsymbol{k})\,k^2 \quad \text{for longitudinal waves}$$
$$\rho\,\omega^2=\mu\,\hat{\alpha}(\boldsymbol{k})\,k^2 \quad \text{for transverse waves}$$

As described previously, in a local continuum, the kernel is a delta function ($\hat{\alpha}(\boldsymbol{k})=1$) in which case the phase velocity (ω/k) does not depend on the wave vector k. For a non-local continuum, the kernel $\hat{\alpha}(\boldsymbol{k})$ provides the means to capture the non linear dependence of phase velocity on the wave vector. In addition, for an isotropic medium, the kernel function does not depend on the mode of wave propagation. This is seen by rewriting the above equation as:

$$\frac{\rho\,\omega_{\mathrm{L}}^2}{\lambda+2\mu}=\frac{\rho\,\omega_{\mathrm{T}}^2}{\mu}=\hat{\alpha}(\boldsymbol{k})\,k^2$$

Here, the subscripts L and T demotes the longitudinal and transverse waves respectively. Phonon dispersion data can be obtained either experimentally or through molecular simulation. The following section assumes that the phonon dispersion is known and focuses on obtaining the two-dimensional (2D) and three-dimensional (3D) kernel in real space ($\alpha_{3D}(\boldsymbol{x})$) from one-dimensional (1D) kernel in reciprocal space ($\hat{\alpha}_{1D}(\boldsymbol{k})$) found by fitting Eq. (4) to the phonon dispersion data.

3. Construction of multidimensional isotropic kernels

Kernel functions needed for 1D elasticity models are even functions, hence can simply be obtained by Fourier-cosine transform of the $\hat{\alpha}_{1D}$. While in 1D, the isotropy induces merely the evenness of the kernel, in 2D and 3D it also induces rotational symmetry, i.e., the $\alpha_{2D}(\boldsymbol{x})$ and $\alpha_{3D}(\boldsymbol{x})$ should have cylindrical and spherical symmetries respectively. The most natural way to build scalar functions on a 3D

domain is through a tensor product along mutually orthogonal directions. For isotropic materials the tensor product scheme may not work, since functions with rotational symmetry may not be separable.[3] There are exceptions, for instance, Gaussian functions are axisymmetric as well as separable. In fact, it is known that every circularly symmetric separable function in 2D is Gaussian (Sahoo, 1990). The following section focuses on a more general technique for the construction of axisymmetric kernel functions.

In case of rotational symmetry of $\alpha_{nD}(\boldsymbol{x})$, its Fourier transform $\hat{\alpha}_{nD}(\boldsymbol{k})$ also proves to be rotationally symmetrical. In other words, the Fourier transform of a radial function is also radial since rotation operation and the Fourier transformation commutes, see appendix B. Here, $\boldsymbol{k}$ is the position vector in the reciprocal space (wave vector). In 2D, the circular symmetry for a function f means

$$f(x_1,x_2)=f^r(r),\quad \text{where } r=(x_1^2+x_2^2)^{1/2} \tag{5}$$

The superscript 'r' refers to radial function. Note that f and f^r are different functions. Its Fourier transform $\hat{f}(k_1,k_2)$ is also circularly symmetric,

$$\hat{f}(k_1,k_2)=\hat{f}^r(k),\quad \text{where } k=(k_1^2+k_2^2)^{1/2} \tag{6}$$

That is the 2-D Fourier transform of a 2-D circularly symmetric function is also circularly symmetric. In addition, the (1D) radial profile of the Fourier transform is identical to the Hankel transform (Bracewell, 1999) of zero order (denoted by $\mathcal{H}_0$) of the radial profile, in the interval $0\leqslant r<\infty$, of the 2-D circularly symmetric function (see appendix B). The relation between these two radial functions is obtained by Hankel transform (also known as Fourier–Bessel transform, see Bracewell (1999)) as

$$\hat{f}^r(k)=\mathcal{H}_0(f^r(r))=2\pi\int_0^\infty f^r(r)J_0(kr)\,r\,dr \tag{7}$$

$$f^r(r)=\mathcal{H}_0^{-1}\left(\hat{f}^r(k)\right)=\frac{1}{2\pi}\int_0^\infty \hat{f}^r(k)J_0(kr)\,k\,dk \tag{8}$$

Note that unlike the Fourier transform there is no change in sign between forward and inverse transform. The coefficients of kr and the factors outside the integrals are consequences of the currently chosen form of the Fourier transform (see Appendix A). Here, J_0 is the zeroth order Bessel function of the first kind,[4] as defined by the following integral equation

$$J_0(x)=\frac{1}{2\pi}\int_{-\pi}^{\pi}e^{\mathrm{i}x\sin\theta}\,\mathrm{d}\theta=\frac{1}{2\pi}\int_0^{2\pi}e^{\mathrm{i}x\cos\theta}\,\mathrm{d}\theta \tag{9}$$

Similarly in 3D the spherical symmetry for a function f yields

$$f(x_1,x_2,x_3)=f^r(r),\quad \text{where } r=(x_1^2+x_2^2+x_3^2)^{1/2} \tag{10}$$

Its Fourier transform $\hat{f}(k_1,k_2,k_3)$ is also spherically symmetric,

$$\hat{f}(k_1,k_2,k_3)=\hat{f}^r(k),\quad \text{where } k=(k_1^2+k_2^2+k_3^2)^{1/2} \tag{11}$$

The relation between these two radial functions is obtained as

$$\hat{f}^r(k)=\mathcal{S}_0(f^r(r))=4\pi\int_0^\infty f^r(r)\,\mathrm{sinc}(kr)\,r^2\,dr \tag{12}$$

$$f^r(r)=\mathcal{S}_0^{-1}\left(\hat{f}^r(k)\right)=\frac{1}{2\pi^2}\int_0^\infty \hat{f}^r(k)\,\mathrm{sinc}(kr)\,k^2\,dk \tag{13}$$

where the $\mathrm{sinc}(x)=\sin(x)/x$ is known as the sinc function Note that the integral of $\mathrm{sinc}(x)$ over $\mathbb{R}$ is not unity, hence it is not normalized. The normalized sinc function is given by $\mathrm{sinc}(x)=\sin(\pi x)/(\pi x)$. The non-normalized sinc function is equal to the first spherical Bessel function of zeroth order $j_0(x)=\sin(x)/x$ (see Arfken et al., 2005, Section 14.2, or Abramowitz, 1972, p. 437, Section 10.1.1). Note that the spherical Bessel function of nth order is related to the Bessel functions of first kind of $(n+1/2)$th order as $j_n(x)=\sqrt{\frac{\pi}{2x}}J_{n+1/2}(x)$, $n=0,1,2,\ldots$ Due to the equality of sinc function to the first spherical Bessel function of zero order, the notation $\mathcal{S}_0$ is used to denote this transformation. The factors outside the integrals for inverse transforms for 2D (Eq. (8)) and 3D (Eq. (13)) can be verified by using the orthogonality relation of Bessel functions (Eq. (21)) and and spherical Bessel functions (Eq. (23)).

3.1. Isotropic kernel construction using known radial profile

In view of the rotational symmetry of the kernels in 2D and 3D, two different routes for the construction of the kernel are explored in the following. In the *first approach*, it is assumed that the radial profiles are identical for different dimensions in the "reciprocal space". In the *second approach*, it is assumed that the radial profiles are identical for different dimensions in the "real space". It will be clear subsequently that kernels obtained on the basis of these two approaches are different in general.

3.1.1. First approach: Identifying reciprocal-space radial-profile for different dimensions

The *first approach* assumes:

$$\hat{\alpha}^r{}_{nD}(k)=c_{nD}\,\hat{\alpha}_{1D}(k),\quad n=2,3 \tag{14}$$

Therefore,

$$\alpha^r_{2D}(r)=c_2\,\mathcal{H}_0^{-1}(\hat{\alpha}_{1D}(k))=\frac{c_2}{2\pi}\int_0^\infty \hat{\alpha}_{1D}(k)J_0(kr)\,k\,dk \tag{15}$$

$$\alpha^r_{3D}(r)=c_3\,\mathcal{S}_0^{-1}(\hat{\alpha}_{1D}(k))=\frac{c_3}{2\pi^2}\int_0^\infty \hat{\alpha}_{1D}(k)\,\mathrm{sinc}(kr)\,k^2\,dk \tag{16}$$

where the constants c_2 and c_3 are used to satisfy the normalization condition.

Normalization of kernel:

In the following the constants c_2 and c_3 are obtain using the normalization conditions

$$2\int_0^\infty \alpha^r_{1D}(r)\,dr=1 \tag{17}$$

$$\int_0^{2\pi}\int_0^\infty \alpha^r_{2D}(r)\,r\,dr\,d\theta=1 \tag{18}$$

$$\int_0^{2\pi}\int_0^{\pi}\int_0^\infty \alpha^r_{3D}(r)\,r^2\sin(\phi)\,dr\,d\phi\,d\theta=1 \tag{19}$$

Note that the factor 2 in Eq. (17) is because the kernel function is even. In multiple dimensions the generalization of the even part of a function is radial part of a function, as used in Eqs. (18) and (19), some more details on this are given in appendix C.

Eq. (18) gives:

$$\frac{1}{c_2}=2\pi\int_0^\infty\left[\frac{1}{2\pi}\int_0^\infty \hat{\alpha}_{1D}(k)J_0(kr)\,k\,dk\right]r\,dr$$
$$=\int_0^\infty\left[\int_0^\infty J_0(kr)\,r\,dr\right]\hat{\alpha}_{1D}(k)\,k\,dk \tag{20}$$

[3] If a function $f(\boldsymbol{x})$ defined on a n-D domain can be written as a tensor product of n functions (along orthogonal directions) defined over real line, as $f(\boldsymbol{x})=f_1(x_1)\otimes f_2(x_2)\otimes\cdots\otimes f_n(x_n)$, then they are called as *separable functions*.

[4] For integer values of n, the nth order Bessel function of the first kind is given by the following integral representation: $J_n(x)=\frac{1}{2\pi}\int_0^{2\pi}e^{-\mathrm{i}(n\tau-x\sin\tau)}\,\mathrm{d}\tau$. For Bessel functions of non-integer order (see Watson, 1995, p. 1976, chapter VI). The Bessel functions arise naturally in Fourier analysis, they are the radial eigenfunctions of the Laplacian operator in polar coordinate.

Bessel functions of first kind satisfy the following orthogonality relationship (see Arfken et al., 2005, Section 14.2)

$$\int_0^\infty J_\alpha(kr)J_\alpha(k'r)\,r\,dr = \frac{1}{k}\delta(k-k') \tag{21}$$

for $\alpha > -1/2$ and $k, k' > 0$. Here δ is Dirac delta function. Noting that $J_0(0) = 1$, yields

$$\int_0^\infty J_0(kr)\,r\,dr = \frac{1}{k}\delta(k)$$

using this relation for the bracketed part of the integrand of Eq. (20) we obtain

$$c_2 = \frac{1}{\hat{\alpha}_{1D}(0)}$$

Similarly for 3D case, Eq. (19) gives:

$$\begin{aligned}\frac{1}{c_3} &= 4\pi\int_0^\infty \alpha^r_{3D}(r)\,r^2\,dr \\ &= 4\pi\int_0^\infty \left[\frac{1}{2\pi^2}\int_0^\infty \hat{\alpha}_{1D}(k)\,\mathrm{sinc}(kr)\,k^2\,dk\right] r^2\,dr \\ &= \frac{2}{\pi}\int_0^\infty \left[\int_0^\infty \mathrm{sinc}(kr)\,r^2\,dr\right]\hat{\alpha}_{1D}(k)\,k^2\,dk\end{aligned} \tag{22}$$

Spherical Bessel functions satisfy the following orthogonality relationship

$$\int_0^\infty j_\alpha(kr)j_\alpha(k'r)\,r^2\,dr = \frac{\pi}{2k^2}\delta(k-k') \tag{23}$$

for $\alpha > -1$ and $k, k' > 0$. noting that $j_0(0) = 1$, yields

$$\int_0^\infty j_0(kr)\,r^2\,dr = \frac{\pi}{2k^2}\delta(k)$$

using this relation for the bracketed term of Eq. (22) we obtain

$$c_3 = \frac{1}{\hat{\alpha}_{1D}(0)}$$

3.1.2. Second approach: Identifying scaled-radial-profile for different dimensions

The *second approach* assumes:

$$\alpha^r_{nD}(r) = C_{nD}\,\alpha^r_{1D}(r), \quad n = 2,3 \tag{24}$$

Therefore in this approach the intended kernel in real space is obtained more directly. However, in this approach the constants (C_{nD}, $n = 2,3$) were needed to ensure normalization of the kernel. The normalization condition for the kernels as given by Eq. (18) and (19) yield the C_{nD}-s as

$$C_{2D} = \frac{1}{2\pi I_{2D}(R=\infty)}, \quad \text{where } I_{2D}(R) = \int_0^R \alpha_{1D}(r)\,r\,dr \tag{25}$$

$$C_{3D} = \frac{1}{4\pi I_{3D}(R=\infty)}, \quad \text{where } I_{3D}(R) = \int_0^R \alpha_{1D}(r)\,r^2\,dr \tag{26}$$

Therefore as the $\hat{\alpha}^r_{1D}(k)$ is provided from the dispersion data, the $\alpha^r_{1D}(r)$ can be obtained via inverse Fourier transform. Subsequently the 2D and 3D kernels are obtained by using normalization constants (C_{nD}, $n = 2,3$). Examples of isotropic kernels in 2D are given in Fig. 1. It shows that these kernels may have singularity at the center, discontinuous derivative, and compact support.

3.2. Connection with the Green's function

The fact that differentiation in the real space gets translated to multiplications in reciprocal domain is advantageous and widely used, in particular for unbounded domain. Let $G(\boldsymbol{x}, \boldsymbol{x}')$ be the

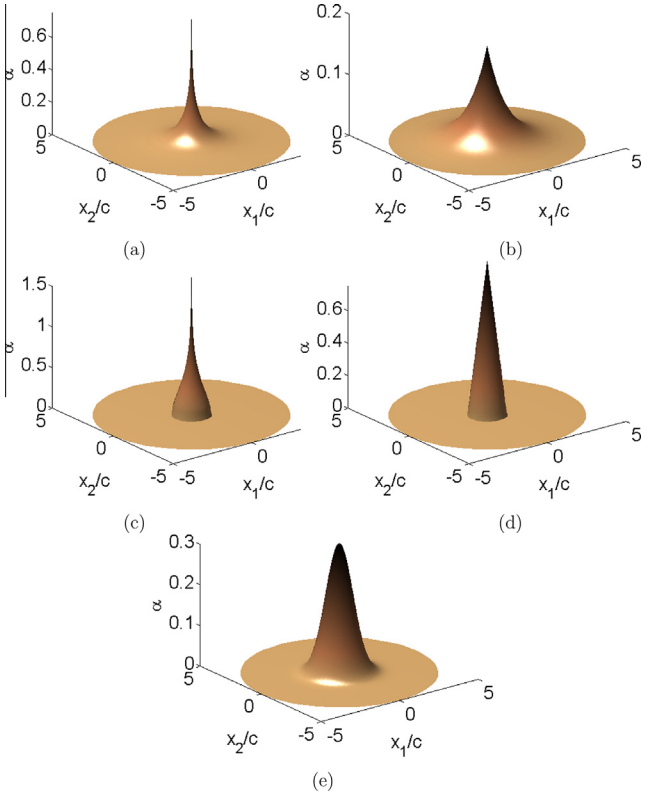

Fig. 1. 2D isotropic kernels: (a,b) stress gradient first and second approach, (c,d) sinc^2 first and second approach, (e) Gaussian (refer to Section 4 for details of the functions $c = 1$ for all kernels). Note that Stress gradient in the first approach and sinc^2 in the first approach have a singularity at the centre.

Green's function for the linear differential operator L in 3D, then $LG(\boldsymbol{x}, \boldsymbol{x}') = \delta(\boldsymbol{x} - \boldsymbol{x}')$. Fourier transform yields $\widehat{G}(\boldsymbol{k}) = 1/\widehat{L}$. Therefore if the 1D kernel $\hat{\alpha}_{1D}(\boldsymbol{k})$ is chosen such that $1/\hat{\alpha}_{nD}(\boldsymbol{k})$ is identical with an arbitrary $\widehat{L}(\boldsymbol{k})$ in n-dimensional space, $n = 1,2,3$, then the kernel becomes the Green function for the operator L. An important consequence for such kernel is that under the operator L the non-local stress yields the local stress. Therefore choosing a kernel is tantamount to choosing a differential operator which transforms the non-local stress to a local one (see Eringen, 1983; Ghosh et al., 2012).

4. Examples

In this section few commonly used functional form of 1D kernels were explored to obtain the 2D and 3D kernels.

4.1. Isotropic non-separable kernel: stress gradient

The 1D kernel $\hat{\alpha}_{1D} = d/(1 + c^2k_1^2)$ corresponds to the *stress gradient theory*. Here, c and d are two constants. The stress gradient theory (Eringen, 1983) relates the nonlocal and classical stresses as $(1 - c^2\nabla^2)\boldsymbol{t} = \boldsymbol{\sigma}$, the corresponding kernel provides a first order approximation to the Born–Kármán model of lattice dynamics. According to the *first approach*, the radial functions in reciprocal space in 1D to 3D is given by $\hat{\alpha}_{nD} = d/(1 + c^2k^2)$, where $k = \|\boldsymbol{k}\|$, $\boldsymbol{k} \in \mathbb{R}^n$, $n = 1,2,3$. Following the *first approach* the radial function for kernels in the real space are

$$\alpha^r_{1D}(r) = \frac{1}{2c}e^{-r/c}, \quad r = |x|, \quad x \in \mathbb{R} \tag{27}$$

$$\alpha^r_{2D}(r) = \frac{1}{2\pi c^2}K_0(r/c), \quad r = \|\boldsymbol{x}\|, \quad \boldsymbol{x} \in \mathbb{R}^2 \tag{28}$$

$$\alpha^r_{3D}(r) = \frac{1}{4\pi c^2 r} e^{-r/c}, \quad r = \|\boldsymbol{x}\|, \ \boldsymbol{x} \in \mathbb{R}^3 \tag{29}$$

where $c > 0$ is a constant and K_0 is the modified Bessel Function of the Second Kind of order zero (see Arfken et al., 2005, Section 14.5, Abramowitz, 1972, p. 376). The integral formula for the modified Bessel function of the second kind of order zero is given as $K_0(r) = \frac{1}{2}\int_0^\infty \mathrm{e}^{-r\cosh t}\,dt$. Later we will need the modified Bessel function of the second kind (of order α), which is given as $K_\alpha(x) = \frac{\pi}{2}\frac{I_{-\alpha}(x) - I_\alpha(x)}{\sin(\alpha\pi)}$; where $I_\alpha(x) = i^{-\alpha}J_\alpha(ix)$ is the Modified Bessel functions of the first kind. In contrast to the oscillating nature of the standard Bessel functions the K_0 is exponentially decaying, that makes it suitable as a kernel function. Note that the 2D kernel given by Eq. (33) is already known (Eringen, 1983, 2002). However, therein it is obtained as Green's function for the differential operator $1 - c^2\nabla^2$. Here, we have provided a systematic approach for 2D and 3D kernel construction from the 1D dispersion data. Given that obtaining Green's functions for an arbitrary operator is difficult, the currently proposed approach is more general. Note that due to the normalization, the constant, d, for $\hat{\alpha}_{1D}$, does not affect the final kernel.

The multi dimensional kernels shows singularity at $r = 0$. Note that these kernels are the Green's function for the operator $1 - c^2\nabla^2$ in 1, 2 and 3 dimensions. Therefore, kernels obtained following the *first approach* corresponds to the Green's function of the stress gradient differential operator. The 1D kernel has jump discontinuity of unit magnitude like a Heaviside function in its derivative at origin. The 2D and 3D kernels have (essential and pole respectively) singularity at origin. Other than the origin they satisfy the homogeneous differential equation $1 - c^2\nabla^2 = 0$. Note the qualitative similarity of the functional form with the Green's function for differential operator in Helmholtz's equation $(\nabla^2 + c^2)$ (Polyanin, 2002; McQuarrie, 2003).

Following the *second approach* the radial function for the kernels in the real space are

$$\alpha^r_{2D}(r) = \frac{1}{2\pi c^2} e^{-r/c}, \quad r = \|\boldsymbol{x}\|, \ \boldsymbol{x} \in \mathbb{R}^2 \tag{30}$$

$$\alpha^r_{3D}(r) = \frac{1}{8\pi c^3} e^{-r/c}, \quad r = \|\boldsymbol{x}\|, \ \boldsymbol{x} \in \mathbb{R}^3 \tag{31}$$

Therefore, the two approaches yield completely different kernels in the real space. While the *first approach* yields only one singularity at $r = 0$ the *second approach* does not have any singularity. Note that all of the required conditions for kernels as mentioned in Section 1 are satisfied by these kernels.

4.2. Isotropic non-separable kernel: sinc^2

The sinc^2 function is another example of a smooth attenuating function that can be used to fit the dispersion data, with the kernel defined as $\hat{\alpha}_{1D} = d\,\mathrm{sinc}^2(kc/2) = \frac{dc^2}{4}\left(\frac{\sin(kc/2)}{k}\right)^2$. Note that the lattice dynamics theory applied to chain of atoms connected by nearest neighbor springs (Born–Kármán model) shows that the phonon dispersion can be expressed in terms of square of the sine function. Using the theory for dispersion in nonlocal elasticity the corresponding kernel turns out to be a sinc^2 function. Following the *first approach* the radial function for the kernels in the real space are

$$\alpha^r_{1D}(r) = \frac{c - r + |c - r|}{2c^2}, \quad r = |x|, x \in \mathbb{R} \tag{32}$$

$$\alpha^r_{2D}(r) = \begin{cases} 0, & \text{for } r > c, \\ \frac{\log\left(\frac{c+\sqrt{c^2-r^2}}{r}\right)}{\pi c^2}, & \text{for } r \leqslant c, \end{cases} \quad r = \|\boldsymbol{x}\|, \ \boldsymbol{x} \in \mathbb{R}^2 \tag{33}$$

$$\alpha^r_{3D}(r) = \frac{1 + \mathrm{sign}(c - r)}{4\pi c^2 r}, \quad r = \|\boldsymbol{x}\|, \ \boldsymbol{x} \in \mathbb{R}^3 \tag{34}$$

Here sign denotes the *sign* function or *signum* function. The one dimensional kernel, α^r_{1D}, is a *triangle* function. For the kernels obtained via *first approach* at $r = 0$ we get a logarithmic singularity (an essential singularity) for α^r_{2D} and a pole for α^r_{3D}. Note that the both α^r_{1D} and α^r_{2D} have discontinuity in their derivative at $r = c$. For α^r_{3D} the *sign* function induces a discontinuity at $r = c$. Note that several numerical strategies are developed to handel discontinuity that may arise due to the singularity present in some of the kernels (see Tornberg, 2002; Muller et al., 2012; Mousavi and Sukumar, 2010).

Following the *second approach* the radial function for the kernels in the real space are

$$\alpha^r_{2D}(r) = \frac{3(c - r + |c - r|)}{2\pi c^3}, \quad r = \|\boldsymbol{x}\|, \ \boldsymbol{x} \in \mathbb{R}^2 \tag{35}$$

$$\alpha^r_{3D}(r) = \frac{3(c - r + |c - r|)}{2\pi c^4}, \quad r = \|\boldsymbol{x}\|, \ \boldsymbol{x} \in \mathbb{R}^3 \tag{36}$$

For this kernel also the two approaches yield completely different kernels in the real space. In this case also the kernels found from the *second approach* do not produce any singularity. For this case, kernels via both approaches in all dimensions are compactly supported over the domain of radius r. It is worth noting that compactly supported kernels would facilitate computational implementation of nonlocal elasticity.

4.3. Isotropic separable kernel: Gaussian

The 1D Gaussian kernel in reciprocal space is, $d\,e^{-c^2k^2/4}$. If the coefficient c is same along different cartesian axes then this is a separable function. For separable axisymmetric functions, construction using tensor product approach and proposed radial function based approach (Section 3) will yield identical kernels. Following the *first approach* the radial function for the kernels in the real space are

$$\alpha^r_{1D}(r) = \frac{e^{-\frac{r^2}{c^2}}}{c\sqrt{\pi}}, \quad r = |x|, \ x \in \mathbb{R} \tag{37}$$

$$\alpha^r_{2D}(r) = \frac{e^{-\frac{r^2}{c^2}}}{c^2\pi}, \quad r = \|\boldsymbol{x}\|, \ \boldsymbol{x} \in \mathbb{R}^2 \tag{38}$$

$$\alpha^r_{3D}(r) = \frac{e^{-\frac{r^2}{c^2}}}{c^3\pi^{3/2}}, \quad r = \|\boldsymbol{x}\|, \ \boldsymbol{x} \in \mathbb{R}^3 \tag{39}$$

The 2D and 3D kernels obtained by *second approach* is identical to the above. Therefore, for 1D Gaussian kernel all approaches yield the same nD kernels.

5. Domain of nonlocal influence and computational kernel

The kernel function for a particular material would depend on the microstructure. Thus, at the atomic scale, it depends both on the spatial distribution of atoms and the interatomic interactions. One of the important feature of kernel is the width/extent of nonlocality. Since, some of the kernels under consideration do not have compact support, the kernels were truncated after some specific radial distances from the center, which is defined as the *computational* radius of influence (r_{comp}), (also known as cut-off radius). The volume covered by the radius of influence is the *computational* compact support (Ω^{comp}) of the kernel. For isotropic materials Ω^{comp} may be taken as a nD ball (spherical volume), $B(r_{\mathrm{comp}})$, of radius r. There is no specific rule to select the radius of influence,

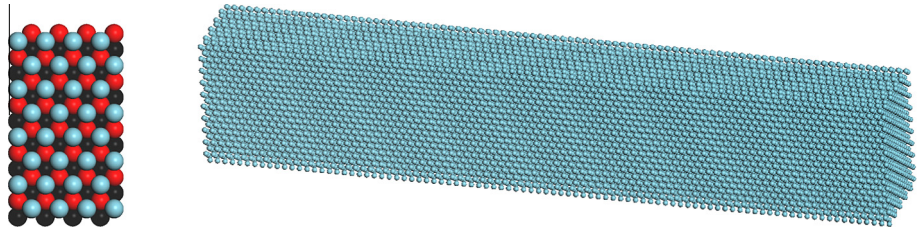

Fig. 2. Molecular model of face centered cubic (FCC) Argon for the tension test and phonon dispersion computation: (left) the hexagonal close pack planes ((111) planes), each color represents a different layer. (right) Long prismatic molecular structure made of 110400 atoms.

however, it is customary to choose the radial distance from the central point to the point where the integral of the kernel reaches some specific value (close to unity). The following function is used to denote integral of the kernel over a nD ball of radius r.

$$w_{nD}(r) = \int_{B(r)} \alpha_{nD}(r)\, dV$$

Using the function $I_{nD}(r)$ defined in Eqs. (25) and (26), for different dimensions, it becomes

$$w_{1D}(r) = 2I_{1D}(r), \quad w_{2D}(r) = 2\pi I_{2D}(r), \quad w_{3D}(r) = 4\pi I_{3D}(r)$$

Analytical expressions for $w_{nD}(r)$ for different dimensions are given in appendix (D). It is not always possible to obtain the analytical expressions for r in terms of the tolerance, hence they have to be obtained numerically from $I_{nD}(r_{\text{comp}})$. For instance, if the tolerance is chosen as 1% (i.e., $w_{3D}(r_{\text{comp}}) = 0.99$), the corresponding radii of influences are given by c, c, 2.382c, 6.64c and 8.41c, for the sinc^2 kernels -1 and -2, Gaussian kernel and Stress Gradient kernels -1 and -2 respectively. We define the computational kernel $\alpha^{\text{comp}}_{nD}$ in the n-Dimension as:

$$\alpha^{\text{comp}}_{nD}(r) = \frac{\alpha_{nD}(r) - \alpha_{nD}(r_{\text{comp}})}{(w_{nD}(r_{\text{comp}}) - \Omega^{\text{comp}}\alpha(r_{\text{comp}}))} \tag{40}$$

The *computational* kernels were set to zero outside their compact support and scaled to satisfy the normalization condition inside their compact support. It is important to note that for a given tolerance, radii of influence are different in different dimensions for the same functional form of the kernel.

6. Modeling size effect observed in molecular simulation through different kernels

Nonlocal theories have advantage over the length-scale-independent classical elasticity theories for capturing the size dependent mechanical properties at small-scale (see Park and Gao, 2006; Maranganti and Sharma, 2007a; Maranganti and Sharma, 2007; Sundararaghavan and Waas, 2011; Wang et al., 2008; Tang and Archive, 2010). In the following, the nonlocal elasticity will be used to phenomenologically demonstrate the size effect for an example case of an Argon single crystal. The available experimental data is at a temperature of 10 K, given in Fig. 3(a) for wave propagation along wave vector [111]. The [111] direction is chosen since the atomic plane has a hexagonal 2D lattice which exhibits in-plane isotropy approximately (see Schargott et al., 2007; Metrikine and Askes, 2006). Using the lattice dynamics theory within the harmonic approximation, the dispersion curve for the direction can be expressed via a sine-function (Dove, 1993) $\omega(k) = \left(\frac{4J_i}{m}\right)^{1/2} \sin(ka/2)$, $ka \in [0, \pi]$. Here, a and m are the inter-planer spacing and mass of atom respectively and J_i, $i = L, T$ is the inter-planer force constant for longitudinal (or transverse) waves. In case of wave propagation along wave vector [111], $a = A/\sqrt{3}$, for longitudinal wave $J_L = 2\bar{k}_0$ and for transversal wave $J_T = \bar{k}_0/2$, here, $\bar{k}_0$ is the interatomic harmonic force constant. The experimental data yields the values for the lattice parameter $A = 5.313$ Å and $\bar{k}_0 \approx 1.32$ (Dove, 1993).

The kernel corresponding to this aforementioned sine curve is the sinc^2 kernel, $\hat{\alpha} = \frac{a^2}{4}\text{sinc}^2(ka/2)$. Note that for the dispersion curve given in Fig. 3(b), the frequency, ω, is scaled with $\left(\frac{4J_i}{m}\right)^{1/2}$, such that, $\bar{\omega} = \omega/\left(\frac{4J_i}{m}\right)^{1/2}$. Owing to the scaling of the experimental data with the initial slope and the in-plane isotropy of the [111] plane, frequencies for longitudinal and transverse waves are almost identical.

We have fitted two other 1D kernels, namely stress gradient and Gaussian, as mentioned in Section 4. We have avoided the best-fit approach since it is more important for physical considerations to fit both the $\bar{\omega}$ (in Hz) and $\frac{\partial\bar{\omega}}{\partial(ka)}$ at the centre and the boundary of Brillouin zone. From the experimental data: $\left.\frac{\partial\bar{\omega}}{\partial(ka)}\right|_{ka=0} = 1/2$, and at the boundary of Brillouin zone $\left.\frac{\partial\bar{\omega}}{\partial(ka)}\right|_{ka=\pi} = 0$. Since the stress

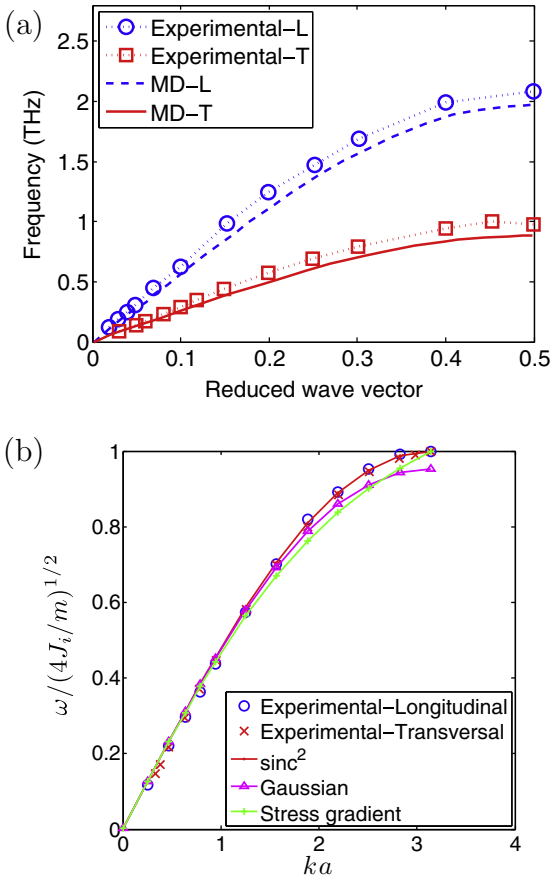

Fig. 3. (a) Comparison of experimental dispersion data for Argon with those computed from MD simulations (Heino, 2007). The experimental data is obtained using a triple-axis neutron spectrometer at 10 K (Fujii et al., 1974). (b) Longitudinal and transversal dispersion curve for FCC argon along the [111] symmetry direction and different curve (1D kernel) fits. Maximum error in the Gaussian kernel fit is ≈5% and in stress gradient kernel is ≈7%.

gradient curve does not show zero slope at the boundary, it is fitted to simply match $\bar{\omega}(k=\pi/a)$. This gives the following 1D stress gradient kernel:

$$\hat{\alpha}(k) = \frac{a^2}{4(1+c^2k^2)}, \quad c = 0.3856a \tag{41}$$

The Gaussian kernel is fitted for zero slope at the boundary of the Brillouin zone, it yields

$$\hat{\alpha}(k) = \frac{a^2}{4} e^{-c^2k^2}, \quad c = 2a/\pi \tag{42}$$

Corresponding $\alpha_{3D}(\boldsymbol{x})$'s for the stress gradient kernels (via first and second approaches) and Gaussian kernels are given by Eqs. (34), (36) and (39), respectively. The radial profile of kernels for the above fitted data are given in Fig. 4. It shows that the two different approaches yield different kernels.

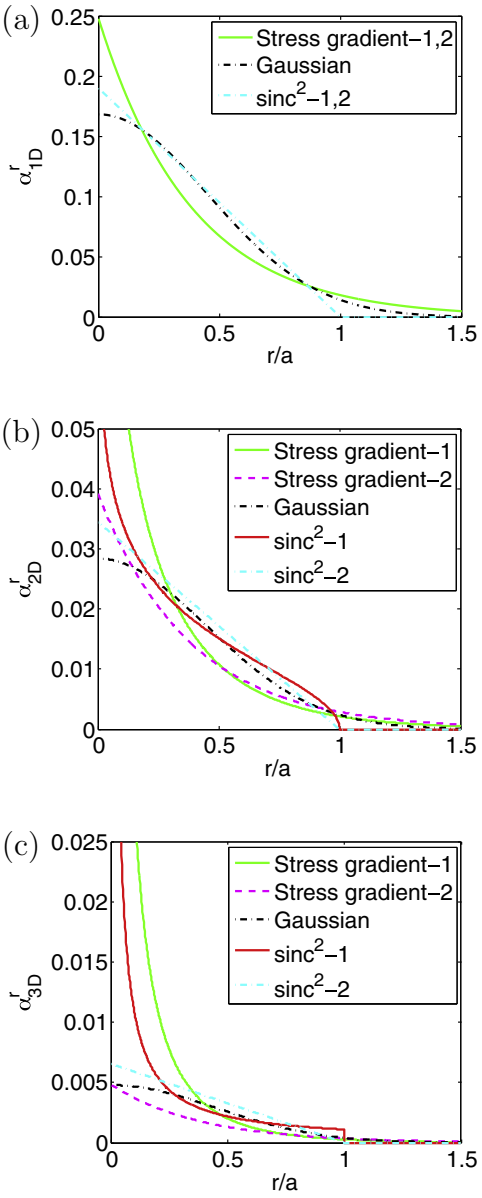

Fig. 4. Radial profile for 1D, 2D and 3D Kernels, given in (a), (b) and (c) respectively. The first and *second approach* for different kernels are denoted by −1 and −2 respectively. Note that for 1D they are same. c is $0.3856a$, $2a/\pi$ and a for stress gradient, gaussian and sinc^2 kernels respectively.

In addition to experimental result shown in Fig. 3 (left), we also plotted the dispersion curve computed using molecular dynamics simulation with a Lennard–Jones potential (Heino, 2007) that closely reproduces the experimental dispersion, we have also verified their MD result. The dispersion is obtained in the MD simulation using the frequency content of the Fourier transformed atomic velocities (for detailed steps see Dickey and Paskin, 1969; Ghosh et al., 2012). To investigate the size dependence of nonlocal energy, we strained this molecular model and computed the nonlocal energies for different sizes of the crystal. An uniform uniaxial tensile strain is imposed along a (prismatic) molecular assembly of length L made of FCC Argon with lattice parameter $A = 5.313$ Å shown in Fig. 2(b). Periodic boundary conditions were imposed along the other directions. The strain can be represented as:

$$\epsilon(\boldsymbol{x}) = \epsilon_0(H(x_1) - H(x_1 - L)) \tag{43}$$

where ϵ_0 is 0.01. H is the Heaviside step function. The internal energy is calculated via atomistic simulations for different L and normalized with that of the initial sample length, 343.7 Å.

The quadratic functional for the nonlocal strain energy density of the body V, under linear small-strain assumption is defined in (Bažant and Jirásek, 2002), as

$$W_{nonlocal} = \frac{1}{2}\int_\Omega \epsilon_{kl}(\boldsymbol{x})\,\alpha(\boldsymbol{x},\boldsymbol{x}')\sigma_{kl}(\boldsymbol{x}')\,d\Omega \tag{44}$$

$$= \frac{1}{2}\epsilon_{kl}(\boldsymbol{x})\,t_{kl}(\boldsymbol{x}) \tag{45}$$

For the nonlocal continuum model the energy per unit length of the prismatic body can be found using Eq. (44). The total energy per unit length is given by

$$En^{NL} = \frac{1}{L}\int_V W_{nonlocal}\,dV = \frac{1}{2L}\int_V \epsilon_{kl}(\boldsymbol{x})\,t_{kl}(\boldsymbol{x})\,dV \tag{46}$$

where V is the volume of the body. The dependence of nonlocal strain energy on the sample size is quantified by the energy ratio

$$\frac{En^{NL}(L)}{En^{NL}(L_0)}$$

The normalized nonlocal energy obtained by nonlocal elasticity and molecular simulations are plotted in Fig. 5. For clarity results only for stress gradient kernels are plotted as it yields the best match among all kernels. The *first* and *second approach* are compared for the popular stress gradient kernel. Both atomistic data and the non-local simulation show a distinct size effect with the energy ratio decreasing with decrease in specimen length. An exact fit is not anticipated due to the cubic anisotropy of the 3D lattice. However, the results indicate that stress gradient kernel through the *second approach* serves as a better fit to molecular data. The reason behind this may be explained using the integral of the kernels, w_{3D}. In Fig. 6 w_{3D}s are plotted for different kernels fitted to the same dispersion curve. It is clear that the stress gradient kernel via *second approach* has the largest radius of influence and captures the longer range interactions seen in the molecular model.[5]

[5] REMARK: Note that the nonlocal energy (given by Eq. (46)) is only function of x_1 only. Hence, for separable kernels calculation of the total nonlocal energy is straight forward. For Gaussian kernel total nonlocal energy as a function of length, L, is given by

$$En^{NL} = \frac{E\epsilon_0^2}{4}\left[\frac{2c}{\sqrt{\pi}}\left(e^{-L^2/c^2}-1\right) + 2L\,\mathrm{Erf}(L/c)\right] \tag{47}$$

where Erf is the error function (see p. 297 of Abramowitz, 1972) given by the integral of the Gaussian distribution: $\mathrm{Erf}(z) = \frac{2}{\sqrt{\pi}}\int_0^z e^{-t^2}dt$.

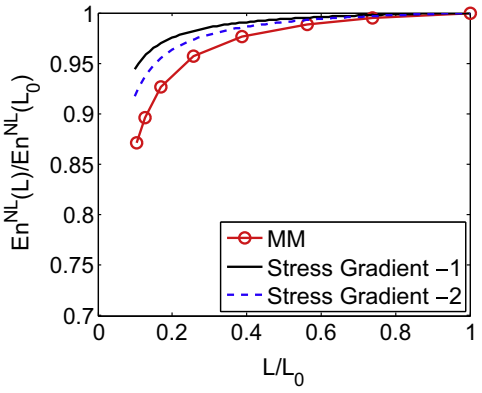

Fig. 5. Comparison of normalized strain energy for different length of molecular structure obtained via molecular mechanics (MM) and nonlocal elasticity with proposed phonon-dispersion-conforming kernels.

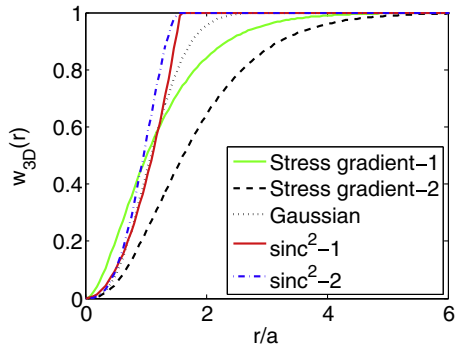

Fig. 6. w_{3D} for different kernels fitted to the dispersion curve given in Fig. 3(b).

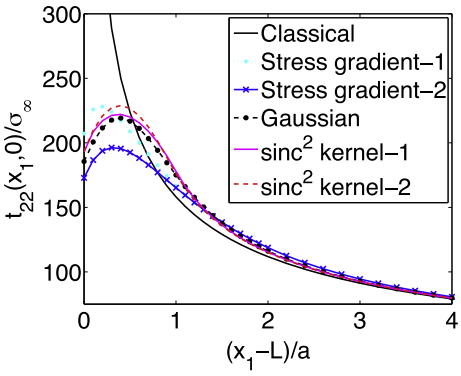

Fig. 7. Comparison of nonlocal hoops stresses along crack-line obtained through different kernels.

7. Effect of kernel on crack-tip stress field

This section demonstrates the sensitivity of the choice of kernel in predicting crack-tip stress fields. Due to the difficulty associated with directly solving the integro-partial differential equilibrium equation for nonlocal elasticity, a Green's function approach proposed in Eringen (1983) is used to obtain the non-local stress field. Here, the equilibrium equation is written as

$$\sigma_{kl,k} + L_G\left(\rho(f_l - \ddot{u}_l)\right) = 0 \tag{48}$$

where $\alpha(r)$ be the Green's function for the operator L_G. It is evident that if $L_G(\rho(f_l - \ddot{u}_l)) = 0$ then the above equation reduces to the classical equilibrium equation: $\sigma_{kl,k} = 0$. The operator L_G can also be applied to the non-local traction boundary conditions, if specified. Therefore a classical boundary value problem is obtained. Solution for such problems are well known through either analytical or numerical techniques. Subsequently the nonlocal stress can be obtained using Eq. (2) (Lu et al., 2007).

Nonlocal stress field is a kernel average of the local stress over a domain, making it finite and smooth even if the stress predicted from local elasticity is singular. The Griffith crack problem is chosen to demonstrate this fact. The *Griffth crack* problem consists of a thin elastic plate, of thickness, t, with a slit crack of length $2L$, $L = 50$ μm, located at $-L \leqslant x_1 \leqslant L$ on x_1-axis, and subjected to a far field uniform tension σ_∞. The crack is assumed to be "mathematically sharp", implying a zero radius of curvature at the tip. The plate dimensions and slit crack length, L are much larger than the plate thickness, t. The 2D stress fields, corresponding to a classical plane stress continuum model are well known, and produces infinite stresses at the crack-tip for classical elasticity. The stress field via classical elasticity is given below:

$$\sigma_{22} = \sigma_\infty\left[\mathrm{Re}\left(\frac{z}{\sqrt{z^2 - L^2}}\right) + x_2\mathrm{Im}\left(\frac{1}{\sqrt{z^2 - L^2}} - \frac{z^2}{\left(z^2 - L^2\right)^{3/2}}\right)\right] \tag{49}$$

where $z = x_1 + ix_2$.

The kernels developed for FCC Argon are used in this example. The nonlocal hoop stresses obtained using various kernels are plotted along the crack-line in Fig. 7. At the crack tip very high stress in front of the crack is weighted along by very low stresses behind the crack, preventing the nonlocal stress from reaching its maximum at the crack-tip. Whereas, slightly away from the crack-tip and in front of it, the local stresses are very high, leading to a maximum in the nonlocal stress. The peak is dependent on the type of kernel, however, maximum difference in the computed results is only $\approx 15\%$. In addition, the peak locations are always within one half of lattice spacing and does not vary widely. The stress-gradient-2 kernel predicts the lowest peak, 197 times σ_∞, due to its wider radius of influence. Other kernels provide similar values for the peak, among them sinc^2 kernels predict highest, close to a stress concentration factor of 229.

We note that in the nonlocal calculation the convolution of the stress with the kernel function is done without considering the crack-boundary effect. Whenever, the intersection of the kernel with the boundary is significant, the ensuing nonlocal stress is not accurate. A better treatment of incorporating boundary effects is needed and that should lead to an improved understanding of the crack-tip nonlocal stress field. However, a key feature of nonlocal theory is the removal of a stress singularity that is non-physical. What is suggested for further investigation is the development of a microstructure specific sub-scale model that can be used in tandem with the non-local model so that a smooth transition from the sub-scale (including boundary regions) towards the interior (away from boundaries) non-local continuum is attained in a rigorous manner. This aspect is left for future study. We note that Molecular Dynamics (MD) calculation of hoop-stress along the crack line has been reported in Jin and Yuan (2005), Yamakov et al. (2006), see for instance Figs. 7 and 8 of Jin and Yuan (2005) and Figs. 8, 9, and 11 of Yamakov et al. (2006). In those studies, the maximum (and finite) stress occurs away from the crack tip, but reasons for this occurrence are not discussed.

8. Conclusions

This paper provides a general approach to obtain multi-dimensional kernels, useful for nonlocal elasticity, from phonon dispersion data. In particular, given a 1D kernel in reciprocal space, the

analytical techniques to obtain the multi-dimensional counterpart for isotropic materials are proposed. For isotropic materials, the kernels obtained must be rotationally symmetric functions in both real as well as in reciprocal space. The present study has proposed two techniques (*first* and *second approach* respectively) to build multi-dimensional kernels such that they have identical radial profile with the 1D kernel in either, the (1) reciprocal space or (2) real space. It is found that for separable functions both approaches become the same. For the *first approach*, the kernels are obtained as the generalized Hankel transform of the radial profile of the kernels in reciprocal space. Multi-dimensional kernels obtained via both approaches are normalized. Using the orthogonality of Bessel functions it is shown that the normalizing factor for the *first approach* is the reciprocal of the slope at the center of the Brillouin zone. Several multi-dimensional analytical kernels are developed. Comparison of nonlocal energy for molecular simulations and nonlocal elasticity with different kernels obtained by fitting dispersion data is used as a test for suitability of these kernels. It turns out that for FCC Argon, stress gradient kernel obtained through the *second approach* provides the closest prediction of the size effect in energy due to a larger zone of influence. Sensitivity of the non-local stress field on the choice of kernel function is analyzed for Griffith's crack problem. It is found that the dependence of (finite) peak stress on kernel function is significant, though the location of the peak is not very sensitive to the choice of the kernel. Since the kernels are derived through atomistic simulations, the corresponding nonlocal stress field obtained is material specific. That makes kernel selection and construction an important part of nonlocal theory development. Any implementation of nonlocal elasticity in multiple dimensions would find this study useful in choosing an appropriate kernel function.

Acknowledgements

The authors are grateful for financial support from the Boeing company and A. Kumar's help with the *perl script*.

Appendix A. Definitions

Let the Fourier transform $\hat{f}$ of an integrable function f defined on $\mathbb{R}^n$

$$\hat{f}(\boldsymbol{k}) = \mathcal{F}(f(\boldsymbol{x})) = \int_{\mathbb{R}^n} f(\boldsymbol{x})\, e^{-i\boldsymbol{x}\cdot\boldsymbol{k}}\, dV_x \tag{50}$$

and

$$f(\boldsymbol{x}) = \mathcal{F}^{-1}(\hat{f}(\boldsymbol{k})) = \frac{1}{(2\pi)^n} \int_{\mathbb{R}^n} \hat{f}(\boldsymbol{k})\, e^{i\boldsymbol{x}\cdot\boldsymbol{k}}\, dV_k \tag{51}$$

where $\boldsymbol{x}\cdot\boldsymbol{k}$ is the dot product of the n-dimensional vectors, $\boldsymbol{x}$ and $\boldsymbol{k}$.

Appendix B. Fourier transform for a radial function

Fourier transform under different transformations (e.g., rotation) has interesting properties and can be found in many text books (see Stein and Weiss, 1971, chapter-IV). A function f defined on $\mathbb{R}^n$ ($n > 1$) is radial if $f(\boldsymbol{x}) = f(\boldsymbol{R}\boldsymbol{x})$ for any orthogonal transformation $\boldsymbol{R}$, ($\boldsymbol{R} \in SO(3)$). This yields that for radial function $f(\boldsymbol{x}) = f(x)$, $x = \|\boldsymbol{x}\|$. In the following we recount that the Fourier transform of a radial function, f, is radial. If $f(\boldsymbol{x})$ and $\hat{f}(\boldsymbol{k})$ are Fourier transform pairs in $\mathbb{R}^n$ then

$$\hat{f}(\boldsymbol{k}) = \mathcal{F}(f(\boldsymbol{x})) = \int_{\mathbb{R}^n} f(\boldsymbol{x})\, e^{-i\boldsymbol{x}\cdot\boldsymbol{k}}\, dV_x = \mathcal{F}(f(\boldsymbol{R}\boldsymbol{x})) = \int_{\mathbb{R}^n} f(\boldsymbol{R}\boldsymbol{x})\, e^{-i\boldsymbol{x}\cdot\boldsymbol{k}}\, dV_x$$

using change of variable $\boldsymbol{y} = \boldsymbol{R}\boldsymbol{x}$ and noting the corresponding Jacobian is one.

$$\hat{f}(\boldsymbol{k}) = \int_{\mathbb{R}^n} f(\boldsymbol{y})\, e^{-i\boldsymbol{R}^{-1}\boldsymbol{y}\cdot\boldsymbol{k}}\, dV_y = \int_{\mathbb{R}^n} f(\boldsymbol{y})\, e^{-i\boldsymbol{y}\cdot\boldsymbol{R}\boldsymbol{k}}\, dV_y = \hat{f}(\boldsymbol{R}\boldsymbol{k})$$

Therefore the Fourier transformed function of a radial function is also radial. In fact using the above it can be shown that the Fourier transform and orthogonal transformation are commutative, i.e., $\mathcal{F}R(f(\boldsymbol{x})) = R\mathcal{F}(f(\boldsymbol{x}))$. Further, the subspace of $L^2(\mathbb{R}^n)$ consisting of all radial functions remains close under Fourier transform.

B.1. Hankel transform in n dimensions

Let f be a radial function defined on $\mathbb{R}^n$ then the Fourier transformed function is also radial and is given by Hankel transform in nD, it has the form

$$\hat{f}(k) = \frac{2\pi}{k^{n/2-1}} \int_0^\infty f(r) J_{n/2-1}(kr)\, r^{n/2} dr \tag{52}$$

Eqs. (7) and (12) are obtained by setting $n = 2$ and $n = 3$ in the above.

Appendix C. Evenness in higher dimensions

A generalization of the even part of a function in more than one dimension is radial part of a function. Eqs. (17)–(19) are corollary of a more general theorem as given below (Baker, 1999):

Theorem. *Let $g : \mathbb{R} \to \mathbb{R}$ be Riemann integrable on $\mathbb{R}$ and let $f(\boldsymbol{x}) = g(r)$, $\forall \boldsymbol{x} \in \mathbb{R}^n$, $r = \|\boldsymbol{x}\|$. Then f is Riemann integrable on $\mathbb{R}^n$ and*

$$\int_{\mathbb{R}^n} f = \omega_{n-1} \int_0^\infty g(r) r^{n-1} dr$$

Theorem. *The area of the unit sphere $S_{n-1} \subseteq \mathbb{R}^n$ is given by $\omega_{n-1} = \frac{2\pi^{\frac{n}{2}}}{\Gamma(\frac{n}{2})}$. Γ is the Gamma function.*

Here S_2, is the standard sphere in 3D, it is a two-dimensional surface of a (three-dimensional) ball in 3D. 1-Sphere, S_1, is the circle in 2D and the 0-sphere, S_0, is the pair of points at the ends of a (one-dimensional) line segment. For S_0 in 1D the two points get count $\omega_0 = 2$. Therefore the area of the 0,1,2 -spheres are given by $2, 2\pi$ and 4π respectively. So they arise in C_{2D} and C_{3D} of Eqs. (25) and (26).

Appendix D. Integral of kernels over a compact support in different dimensions

Analytical expressions for the integral of kernels over the compact support is given below for all the kernels. Here r_{cut} denotes cut-off distance mesured in different dimensions.

For Gaussian kernels:

$$w_{1D}(r_{\text{cut}}) = \text{Erf}\left(\frac{r_{\text{cut}}}{c}\right)$$

$$w_{2D}(r_{\text{cut}}) = 1 - e^{\frac{r_{\text{cut}}^2}{c^2}}$$

$$w_{3D}(r_{\text{cut}}) = 4\pi\left(-\frac{e^{\frac{r_{\text{cut}}^2}{c^2}} r_{\text{cut}}}{2c\pi^{3/2}} + \frac{\text{Erf}\left(\frac{r_{\text{cut}}}{c}\right)}{4\pi}\right)$$

Here, Erf is the error function.

For stress gradient kernels via first approach:

$$w_{1D}(r_{\text{cut}}) = 1 - e^{-\frac{r_{\text{cut}}}{c}}$$

$$w_{2D}(r_{\text{cut}}) = \frac{c - r_{\text{cut}}\,\mathrm{K}_1\left(\frac{r_{\text{cut}}}{c}\right)}{c}$$

$$w_{3D}(r_{\text{cut}}) = \frac{c - e^{-\frac{r_{\text{cut}}}{c}}(c + r_{\text{cut}})}{c}$$

Here, K_1 is the modified Bessel Function of the Second Kind of order one.

For stress gradient kernels via second approach:

$$w_{2D}(r_{\text{cut}}) = 1 - e^{-r_{\text{cut}}}(1 + r_{\text{cut}})$$

$$w_{3D}(r_{\text{cut}}) = \frac{1}{2}(2 - e^{-r_{\text{cut}}}(2 + r_{\text{cut}}(2 + r_{\text{cut}})))$$

For sinc kernels via first approach:

$$w_{1D}(r_{\text{cut}}) = \begin{cases} 1 & r_{\text{cut}} > c \\ \frac{2c\,r_{\text{cut}} - r_{\text{cut}}^2}{c^2}, & \text{Otherwise} \end{cases}$$

$$w_{2D}(r_{\text{cut}}) = \begin{cases} 1 & r_{\text{cut}} > c \\ \frac{c\left(c - \sqrt{c^2 - r_{\text{cut}}^2}\right) + r_{\text{cut}}^2 \log\left(\frac{c + \sqrt{c^2 - r_{\text{cut}}^2}}{r_{\text{cut}}}\right)}{c^2}, & \text{Otherwise} \end{cases}$$

$$w_{3D}(r_{\text{cut}}) = \begin{cases} 1 & r_{\text{cut}} > c \\ \frac{r_{\text{cut}}^2}{c^2}, & \text{Otherwise} \end{cases}$$

For sinc kernels via second approach:

$$w_{2D}(r_{\text{cut}}) = \begin{cases} 1 & r_{\text{cut}} > c \\ \frac{3c\,r_{\text{cut}}^2 - 2r_{\text{cut}}^3}{c^3}, & \text{Otherwise} \end{cases}$$

$$w_{3D}(r_{\text{cut}}) = \begin{cases} 1 & r_{\text{cut}} > c \\ \frac{4c\,r_{\text{cut}}^3 - 3r_{\text{cut}}^4}{c^4}, & \text{Otherwise} \end{cases}$$

References

Abramowitz, M. (Eds.), 1972. I.A. Stegun. 9.6 in Handbook of Mathematical Functions with Formulas, Graphs, and Mathematical Tables, 9th printing. Dover, New York.

Aifantis, E.C., 2003. Update on a class of gradient theories. Mech. Mater. 35 (3–6), 259–280.

Arfken, G.B., Weber, H.J., Harris, F., 2005. Mathematical Methods For Physicists. Elsevier Science. ISBN 9780120598762.

Askes, H., Aifantis, E.C., 2011. Gradient elasticity in statics and dynamics: an overview of formulations, length scale identification procedures, finite element implementations and new results. Int. J. Solids Struct. 48 (13), 1962–1990.

Baker, J.A., 1999. Integration of radial functions. Math. Mag. 72 (5), 392–395.

Bažant, Z.P., Cedolin, L., 2010. Stability of Structures: Elastic, Inelastic. World Scientific Fracture and Damage Theories.

Bažant, Z.P., Chang, Ta-Peng, 1984. Instability of nonlocal continuum and strain averaging. J. Eng. Mech. 110 (10), 1441–1450.

Bažant, Z.P., Jirásek, M., 2002. Nonlocal integral formulations of plasticity and damage: survey of progress. J. Eng. Mech. ASCE 128 (11), 1119–1149.

Borino, G., Failla, B., Parrinello, F., 2003. A symmetric nonlocal damage theory. Int. J. Solids Struct. 40 (13–14), 3621–3645.

Bracewell, R.N., 1999. In The Fourier Transform and Its Applications, third ed. McGraw-Hill, New York.

Dickey, J.M., Paskin, A., 1969. Computer simulation of the lattice dynamics of solids. Phys. Rev. 188, 1407–1418.

Dove, M.T., 1993. Introduction to Lattice Dynamics. Cambridge University Press, 1993.

Eringen, A.C., 1983. On differential equations of nonlocal elasticity and solutions of screw dislocation and surface waves. J. Appl. Phys. 54 (9), 4703–4710.

Eringen, A.C., 2002. Nonlocal Continuum Field Theories. Springer.

Fujii, Y., Lurie, N.A., Pynn, R., Shirane, G., 1974. Inelastic neutron scattering from solid ^{36}Ar. Phys. Rev. B 10, 3647–3659.

Ghosh, S., Kumar, A., Waas, A.M., Sundararaghavan, V., 2012. Non-local modeling of epoxy using an atomistically-informed kernel. Int. J. Solids Struct. 50 (19), 2837–2845.

Ghosh, S., Sundararaghavan, V., Waas, A.M., 2013. Construction of kernel for nonlocal elasticity from one-dimensional dispersion data in reciprocal space. In: 54th AIAA/ASME/ASCE/AHS/ASC Structures, Structural Dynamics, and Materials Conference and Co-located Events, 8–11, Boston, Massachusetts. American Institute of Aeronautics and Astronautics, Inc., April 2013, pp. 1508–1509.

Han, C-S., 2010. Influence of the molecular structure on indentation size effect in polymers. Mater. Sci. Eng. A 527, 619–624.

Heino, P., 2007. Dispersion and thermal resistivity in silicon nanofilms by molecular dynamics. Eur. Phys. J. B 60, 171–179.

Jin, Y., Yuan, F.G., 2005. Nanoscopic modeling of fracture of 2D graphene systems. J. Nanosci. Nanotechnol. 5 (4), 601–608.

Lam, D.C.C., Yang, F., Chong, A.C.M., Wang, J., Tong, P., 2003. Experiments and theory in strain gradient elasticity. J. Mech. Phys. Solids 51 (8), 1477–1508.

Lu, Pin, Zhang, P.Q., Lee, H.P., Wang, C.M., Reddy, J.N., 2007. Non-local elastic plate theories. Proc. Roy. Soc. A: Math. Phys. Eng. Sci. 463 (2088), 3225–3240.

Maranganti, P., Sharma, R., 2007. Length scales at which classical elasticity breaks down for various materials. Phys. Rev. Lett. 98 (19), 195504.

Maranganti, P., Sharma, R., 2007a. A novel atomistic approach to determine strain-gradient elasticity constants: Tabulation and comparison for various metals, semiconductors, silica, polymers and the (ir) relevance for nanotechnologies. J. Mech. Phys. Solids 55 (9), 1823–1852.

Maugin, G.A., Metrikine, A.V. (Eds.), 2010. Mechanics of Generalized Continua: One Hundred Years After the Cosserats, vol. 10. Springer, New York.

McQuarrie, D.A., 2003. Mathematical Methods for Scientists and Engineers. University Science Books, Sausalito, California.

Metrikine, A.V., Askes, H., 2006. An isotropic dynamically consistent gradient elasticity model derived from a 2d lattice. Philos. Mag. 86 (21–22), 3259–3286.

Mousavi, S.E., Sukumar, N., 2010. Generalized Gaussian quadrature rules for discontinuities and crack singularities in the extended finite element method. Comput. Meth. Appl. Mech. Eng. 199 (49–52), 3237–3249.

Muller, B., Kummer, F., Oberlack, M., Wang, Y., 2012. Simple multidimensional integration of discontinuous functions with application to level set methods. Int. J. Numer. Meth. Eng. 92 (7), 637–651.

Park, S.K., Gao, X-L., 2006. Bernoulli euler beam model based on a modified couple stress theory. J. Micromech. Microeng. 16 (11), 2355–2359.

Picu, R.C., 2002. On the functional form of non-local elasticity kernels. J. Mech. Phys. Solids 50 (9), 1923–1939.

Polizzotto, C., 2001. Nonlocal elasticity and related variational principles. Int. J. Solids Struct. 38 (42–43), 7359–7380.

Polizzotto, C., Fuschi, P., Pisano, A.A., 2004. A strain-difference-based nonlocal elasticity model. Int. J. Solids Struct. 41 (910), 2383–2401.

Polyanin, A.D., 2002. Handbook of Linear Partial Differential Equations for Engineers and Scientists. Chapman & Hall/CRC.

Sahoo, P.K., 1990. Circularly symmetric separable functions are gaussian. Appl. Math. Lett. 3 (3), 111–113.

Schargott, M., Popov, V.L., He, M., 2007. Macroscopic isotropy of two- and three-dimensional elastic lattice models. Tribol. Int. 40 (6), 937–941.

Stein, E.M., Weiss, G., 1971. Fourier Analysis on Euclidean Spaces. Princeton Mathematical Series, no. 31, Princeton University Press, Princeton.

Sundararaghavan, V., Waas, Anthony, 2011. Non-local continuum modeling of carbon nanotubes: physical interpretation of non-local kernels using atomistic simulations. J. Mech. Phys. Solids 59 (6), 1191–1203.

Tang, C., Alici, G., 2010. Investigation of the size effects in timoshenko beams based on the couple stress theory. Archive of Applied Mechanics, 2010.

Tornberg, A.-K., 2002. Multi-dimensional quadrature of singular and discontinuous functions. BIT Numer. Math. 42, 644-669. ISSN 0006-3835.

Wang, Q., Han, Q.K., Wen, B.C., 2008. Estimate of material property of carbon nanotubes via nonlocal elasticity. Adv. Theor. Appl. Mech. 1 (1), 1–10.

Watson, G.N., 1995. A Treatise on the Theory of Bessel Functions. Cambridge University Press, 1995.

Yamakov, V., Saether, E., Phillips, D.R., Glaessgen, E.H., 2006. Molecular-dynamics simulation-based cohesive zone representation of intergranular fracture processes in aluminum. J. Mech. Phys. Solids 54, 1899–1928.